Proceedings of the ASME 2007 International Design Engineering Technical Conferences & Computers and Information in Engineering Conference
IDETC/CIE 2007
September 4-7, 2007, Las Vegas, Nevada, USA

DETC2007-35226

TAILORING OF TWO-DIMENSIONAL BAND-GAP MATERIALS FOR BROADBAND FREQUENCY ISOLATION

Mahmoud I. Hussein[*1]
Department of Engineering
Gregory M. Hulbert[2]
Department of Mechanical Engineering
Karim Hamza[2]
Department of Mechanical Engineering
Kazuhiro Saitou[2]
Department of Mechanical Engineering

[1]University of Cambridge
Trumpington Street, Cambridge CB2 1PZ, U.K.
[2]University of Michigan
2350 Hayward, Ann Arbor, Michigan 48109-2125 U.S.A.

ABSTRACT

The spatial distribution of material phases within a periodic composite can be engineered to produce band gaps in its frequency spectrum. Applications for such composite materials include vibration and sound isolation. Previous research focused on utilizing topology optimization techniques to design two-dimensional periodic materials with a maximized band gap around a particular frequency or between two particular dispersion branches. While sizable band gaps can be realized, the possibility remains that the frequency bandwidth of the load that is to be isolated might significantly exceed the size of the band gap. In this paper, genetic algorithms are used to design squared bi-material unit cells with a maximized sum of relative band-gap widths over a prescribed frequency range of interest. The optimized unit cells therefore exhibit broadband frequency isolation characteristics. The effects of the ratios of contrasting material properties are also studied. The designed cells are subsequently used, with varying levels of material damping, to form a finite vibration isolation structure, which is subjected to broadband loading conditions. Excellent isolation properties of the synthesized material are demonstrated for this structure.

1. INTRODUCTION

Wave propagation in heterogeneous media is dispersive, i.e., the media causes an incident wave to decompose into multiple waves with different frequencies. A medium with periodic heterogeneity has distinct frequency ranges in which waves are either effectively attenuated or allowed to propagate in space. These frequency ranges are referred to as *stop bands* (or band gaps) and *pass bands* (or bands), respectively, and are attributed to mechanisms of wave interferences within the scattered elastic field. From a practical perspective, it has been shown that under certain conditions bounded structures formed from periodic materials can exhibit similar frequency-banded wave motion characteristics (e.g., [1-4]).

By controlling the layout of constituent material phases and the ratio of their properties within a unit cell, a periodic composite can be designed to have a desired frequency band structure (the size and location of stop bands and pass bands). In this study the interest is in the design of periodic bi-material composites capable of isolating a broadband vibration load or sound signal. Thus the goal is to generate unit cells with a maximized sum of band-gap frequency ranges spanning the first few dispersion branches. Since it is desirable to keep the branches low to access the low frequency content of a generic broadband load, the design objective is modified such that the sum of the *relative* band-gap frequency ranges is minimized. A relative band gap frequency range is defined as the band-gap width divided by its central frequency. Similar studies are available in the literature with a focus on maximizing a single band gap [5-8], or multiple band gaps in the context of 1D problems [9,10].

An evolutionary optimization technique, namely genetic algorithms (GA), is chosen for the unit cell optimization problem. GA is advantageous for this type of problem because it simultaneously evolves multiple designs and eventually converges (with high probability) to near-global optimality. A unit cell (chosen to be squared in shape) is discretized into a uniform grid of pixels with the design variables being the material type of each pixel represented as a zero-one binary variable, where "zero" denotes one material type (the denser and stiffer phase) and "one" denotes the other (the less dense and less stiff phase). This choice of design variable leads to a zero-one integer programming formulation. In this manner, a string of binary variables controls both the volume fractions

[*] Research Associate and author of correspondence, Phone: +44 (0)1223 332-781, Fax: +44 (0)1223 332-662, Email: mih21@cam.ac.uk.

and distributions of the two constituent materials within the unit cell. The materials considered are linear elastic and isotropic, and the model studied is that of out-plane wave motion. The frequency band diagrams for the designs are computed using Floquet-Bloch theory and the finite element method [e.g., 3,6,11,12].

The above optimization process is carried out for a range of material pairs with the ratio of Young's moduli, E_r, ranging from 1 to 8, and the ratio of densities, ρ_r, ranging from 1 to 4 (i.e., a total of 31 possibilities omitting the $E_r=1/\rho_r=1$ case).

To test the vibration isolation performance of an optimal material in a finite structural setting, an initial boundary value problem (IBVP) is solved for a partially clamped structure (composed from the optimal material) that is subjected to a broadband double Gaussian displacement excitation. As an example, the optimal design for the $E_r=8$ and $\rho_r=4$ case is employed, and the excitation load is chosen to span in frequency all the dispersion branches considered in the unit cell optimization process. The finite element method and explicit time integration are used to obtain the solution of the IBVP. Proportional material damping is also introduced and its effect on the maximum transmitted response is quantified. Finally, comparisons are made with a totally homogeneous structure composed from the stiff/heavy material and another composed from the compliant/light material.

In the next section, the mathematical and numerical formulation for computing band diagrams is described, as well as a brief presentation of the structural analysis equations. In Section 3, the binary formulation is presented along with a description of the employed genetic algorithm. Section 4 presents the results for both the unit cell and structure problems. Finally conclusions remarks are drawn in Section 5.

2. DISPERSIVE WAVE MOTION IN PERIODIC MATERIALS AND STRUCTURES

2.1. Unit Cell Analysis

The governing equation for the elastodynamics of a linear isotropic, heterogeneous medium is

$$\nabla(\lambda+\mu)\nabla\cdot\mathbf{u}+\nabla\cdot\mu\nabla\mathbf{u}=\rho\ddot{\mathbf{u}} \tag{1}$$

where $\mathbf{u}$ represents the displacement solution field, the parameters λ and μ are the Lamé constants, ∇ denotes the gradient operator, and a superposed dot denotes differentiation with respect to time t. Defining the unit coordinates as x, y and z, $\mathbf{u}^{\mathrm{T}}=(u, v, w)$, where u, v and w denote the displacement along these coordinate directions, respectively. Considering plane wave propagation along the x-y plane, and narrowing attention to out-of-plane polarization (i.e., transverse *SH* waves), Eq. (1) reduces to

$$\frac{\partial}{\partial x}\left(\mu\frac{\partial w}{\partial x}\right)+\frac{\partial}{\partial y}\left(\mu\frac{\partial w}{\partial y}\right)=\rho\frac{\partial^2 w}{\partial t^2}. \tag{2}$$

In this study, a two-dimensional periodic medium will be characterized by an infinitely repeated unit cell Y, where Y represents a square domain as shown in Fig. 1. Within this domain, Eq. (2) has a Floquet-Bloch solution of the form

$$w(\mathbf{y},\mathbf{k};t)=\tilde{w}e^{i\mathbf{k}^{\mathrm{T}}\mathbf{y}}e^{i\omega t}, \tag{3}$$

where $\tilde{w}$ is Y-periodic, $\mathbf{y}=(x, y)$, and $\mathbf{k}=(k_x, k_y)$ is the wave vector. Substituting Eq. (3) into Eq. (2) leads to the following transform

$$\nabla\rightarrow\nabla+i\mathbf{k}. \tag{4}$$

For *SH* waves, the resulting strong form is (dropping the tilda)

$$(\nabla+i\mathbf{k})\cdot\frac{\mu}{\rho}(\nabla+i\mathbf{k})w+\omega^2 w=0, \tag{5}$$

while the weak form is

$$\int_{\mathrm{Y}}\left[\overline{(\nabla+i\mathbf{k})v}\cdot\frac{\mu}{\rho}(\nabla+i\mathbf{k})w+\omega^2\bar{v}w\right]\mathrm{dY}=0. \tag{6}$$

Both operators in Eq. (6) are Hermitian by construction. The Galerkin method is then used to obtain the following algebraic problem

$$(\mathbf{K}(\mathbf{k})-\omega^2\mathbf{M})w=0 \quad \text{in Y}, \tag{7}$$

which can be solved for the frequencies $\omega_i(\mathbf{k})$, $i=1,\ldots,n_d$, where n_d denotes the number of degrees of freedom. Further details of this approach are provided by Hussein et al. [3]. Perioidic boundary conditions are applied on Y.

Equation (7) is solved for wave vector $\mathbf{k}$ spanning the first Brillouin zone $\mathbf{k}\in[-\pi, \pi]^2$ over the unit cell, but with the utilization of symmetry it is sufficient for $\mathbf{k}$ to cover the irreducible Brillouin zone (see [13]) as shown in Fig. 1. Following common practice, the search space is narrowed even further to only considering the wave vectors pointing to positions along the border of this zone (triangle shown in Fig. 1), that is, end points along the paths $\Gamma\rightarrow$X, X$\rightarrow$M and M$\rightarrow\Gamma$. This process generates representative dispersion curves (frequency versus wave vector) for the periodic medium. In recent years, several methods have been developed for computing frequency band diagrams for periodic media. In this paper, the standard finite element method [e.g., 3,6,11,12] is used to solve the variational eigenvalue problem, in Galerkin form, given in Eq. (7). For computational purposes, $\omega_i(\mathbf{k})$ is only evaluated at a discrete (uniformaly distributed) set of points n_k along the entire border of the irreducible Brillioun zone. The discrete wave vector set is denoted $\mathbf{k}_j=[k_1,k_2]_j$, $j=1,\ldots,n_k$.

To highlight this process, consider the arbitrarily chosen periodic material design shown in Fig. 2a. The unit cell in this design is composed of a compliant (matrix) material "m" (shown in white), and a contrasting stiff (fiber) material "f" (shown in black). The compliant material is chosen to have a Young's modulus, E_m, of 4 GPa, and density, ρ_m, of 1000 kg/m^3. The stiff material is chosen such that $E_r=E_f/E_m=8$ and $\rho_r=\rho_f/\rho_m=4$. The frequency spectrum for out-of-plane wave motion for this configuration is shown in Fig. 2b. The non-dimensional frequency

$$\Omega=\omega d/(E_m/\rho_m)^{1/2}, \tag{8}$$

and the non-dimensional wave vector

$$\boldsymbol{\xi} = d \cdot \mathbf{k} \tag{9}$$

define the ordinate and abscissa, respectively. The first, second and third vertical segments of the plot (separated by dotted lines) represent wave vectors pointing to positions along Γ→X, X→M and M→Γ, respectively. Only two narrow band gaps exist over the displayed frequency range for this design.

2.2. Structural Analysis

For the bounded structure problem, Eq. (1) is transformed to the following algebraic equation using a standard finite element method:

$$\mathbf{M}\ddot{\mathbf{D}} + \mathbf{C}\dot{\mathbf{D}} + \mathbf{K}\mathbf{D} = \mathbf{F}\,, \tag{10}$$

where **M, C** and **K** are the stiffness, damping and consistent mass matrices, respectively, and **D** and **F** are the nodal displacement and force vectors, respectively. The type of damping considered is discussed later. In this study, the time dependent set of ordinary differential equations, Eq. (10), with appropriate boundary and initial conditions are solved using the standard explicit central difference scheme. In the integration process, a stable solution is obtained if the discrete time step (denoted Δt) is chosen to be less or equal to the Courant-Friedricks-Levy (CFL) number throughout the finite element mesh, i.e., $\Delta t = h^e / c_p^{(j)}$ where h^e denotes size of element e and $c_p^{(j)}$ denotes out-of-plane shear wave speed for the material phase "j" occupying element e.

3. OPTIMIZATION OF BAND-GAP MATERIAL

3.1. Unit Cell Design Problem Formulation

The square unit cell Y is composed of $n_l \times n_l$ pixels forming a matrix **G**. Each of the pixels can be either assigned the stiff/heavy material (fiber) or the compliant/light one (matrix). Varying the distribution of these material phases within the unit cell allows for shaping the frequency spectrum of the periodic medium. In this manner, designs can be generated to achieve a target dynamical performance. Details of the measure for the performance are given in Section 4. The general form of the cell design problem is given as:

$$\text{Maximize } f = \mathit{Perfomance}(\mathbf{G})\,, \tag{11}$$

where $\mathbf{G} = \{g_{ij}\} : i, j = 1,..., n_l$ is an $n_l \times n_l$ binary matrix, with $g_{ij} \in \{0,1\}$. When $g_{ij} = 1$, the fiber material is assigned to the pixel ij, and when $g_{ij} = 0$, the matrix material is assigned to the pixel ij.

Since the chosen type of material periodicity enforces symmetry about both axes and the diagonals, the lower triangle of one quarter of the matrix **G** is a sufficient representation of all the independent decision variables in **G**. Thus, the optimization problem can be re-written as

$$\text{Maximize } f = \mathit{Perfomance}(\mathbf{b})\,, \tag{12}$$

where $\mathbf{b} \in \{0,1\}^{n_{\text{var}}}$ is the vector of independent decision variables in the matrix **G** and n_{var} is the number of independent decision variables. When n_l is an even number (as adopted in this study),

$$n_{\text{var}} = \frac{n_l(n_l+2)}{8}\,. \tag{13}$$

3.2. Genetic Algorithm

The objective function of the general case of the cell design problem is rarely guaranteed to be unimodal with respect to the design variables. Thus local search based optimization can easily get trapped at a local optimum that is short of the best achievable performance. Furthermore, for a practical unit cell resolution the number of independent decision variables is excessively large to allow exhaustive enumeration. For example, the results in this paper are generated via a unit cell of $n_l = 20$ (20×20 pixels), which has 55 independent decision variables. Exhaustive enumeration would require $2^{55} \approx 3.6 \times 10^{16}$ objective evaluations.

To overcome the above limitations, a genetic algorithm [14] is employed in this study. A genetic algorithm is a heuristic optimization technique that attempts to mimic the process of natural evolution. Studies in the literature have shown genetic algorithms to be capable of tackling difficult problems and generating near-global optimal solutions [14, 15]. The steps of the adopted algorithm are described as follows:

1. Create a population *P* of *p* random designs and evaluate their objective function values. Also create empty set *Q*.
2. Pass a copy of the best design in *P* to *Q*.
3. Select two designs g_i and g_j in *P* via binary tournament selection [15].
4. Crossover g_i and g_j to generate new design(s) with a certain probability. Since the decision variables in the vector **b** can be nonlinearly dependent, a geometric graph based crossover [16] is employed.
5. Mutate the new design(s) with a certain probability.
6. Evaluate the objective function values of the new design(s) and store in *Q*. If the size of *Q* is less than *p*, go to 3.
7. Replace *P* with *Q*, empty *Q*, and increment the generation coun-

ter. If the generation counter has reached a pre-specified number, terminate the process. Otherwise go to 2.

8. Run a short local search from the best design in *P* to fine-tune the result. The local search is performed by accepting a new design only if a single bit flip of the vector **b** produces a better design.

4. OPTIMIZATION STUDIES

4.1. Objective Function and Optimal Unit Cell Designs

The objective is to design a unit cell consisting of two contrasting material phases and whose frequency spectrum exhibits multiple band gaps with the sum of their relative widths maximized. The considered frequency range of interest is the range spanning the first six dispersion branches. From a practical perspective, a finite structure composed of several cells of such a design could be used to attenuate the propagation of a broadband shock or sound pulse [4,10,12], as will be demonstrated in Section 4.2.

With such target dynamical characteristics in mind, the objective function is specifically defined as the sum of the widths to central frequency ratio of the first five band gaps (if any). The objective is numerically evaluated for a given design **b** of the unit cell using the finite element method as described earlier. The equation for the objective is given as

Maximize:

$$f(\mathbf{b}) = \sum_{i=1}^{5} \frac{max(min_{j=1}^{n_k}(\omega_{i+1}^2(\mathbf{k}_j,\mathbf{b})) - max_{j=1}^{n_k}(\omega_i^2(\mathbf{k}_j,\mathbf{b})))}{(min_{j=1}^{n_k}(\omega_i^2(\mathbf{k}_j,\mathbf{b})) + max_{j=1}^{n_k}(\omega_{i+1}^2(\mathbf{k}_j,\mathbf{b})))/2}, \quad (14)$$

where $min_{j=1}^{n_k}(\omega_i^2(\mathbf{k}_j,\mathbf{b}))$ and $max_{j=1}^{n_k}(\omega_i^2(\mathbf{k}_j,\mathbf{b}))$ denote the minimum, and maximum, respectively, of the *i*th eigenvalue over the entire discrete wave vector set. When the minimum of the *i*+1th eigenvalue is greater than the maximum of the *i*th eigenvalue, a band gap exists; otherwise no band gap exists and the *i*th term in the objective is equal to zero.

The genetic algorithm described in Section 3.2 was applied to this problem using the execution parameters given in Table 1. Final tuning of the cell design was attained by running local search as mentioned earlier. In all cases, the local search converged in only two to three iterations, which indicates that the genetic algorithm arrived close to an optimum.

The optimization process mentioned above was carried out for a range of material properties (i.e., Young's modulus ratio and density ratio) to gain insights into the effects of the material property ratios on the topology and objective value of the optimal designs. Fig. 3 shows a matrix of optimal designs (shown in the form of 3x3 unit cells) for the value of E_r ranging from 1 to 8, and the value of ρ_r ranging from 1 to 4 (i.e., a total of 31 possibilities omitting the homogeneous case of E_r=1/ρ_r=1). It is challenging to extract any particular pattern from this *design mosaic* other than that the lower contrast cases consist of hollow fiber phase "reinforcements" while the higher contrast cases produce solid "reinforcements". Clearly the evolution of the optimal topology with varying material contrasts is qualitative in nature. The corresponding dispersion curves are shown in Fig. 4. Most apparent is the expected increase in the total band gap frequency ranges with increasing material contrasts. Less intuitive is how the optimal design band diagrams transform from single to double, and subsequently to triple, band-gaps as the material contrasts increase. In particular, an increase in density ratio tend to be more effective in producing multiple gaps than an increase in the Young's modulus which is effective in producing wide single gaps. Finally, the objective values for the optimal design is plotted as a function of material property ratios in Fig. 5. The objective is observed to increase almost linearly with E_r and ρ_r with the rate of increase with E_r growing as ρ_r is increased and vice versa. In the same figure, dashed curves are included to represent an evaluation of the objective function based on the optimal design for E_r=4 and ρ_r=4 (i.e., Design A in the figure, which is associated with the best reported objective value). These curves show that the optimal design is strongly dependent on the material ratios, which is attributed to the inherent complexities of the band-gap generating interference mechanisms within the scattered wave fields.

4.2. Performance of Structure Composed of Optimal Band-Gap Material

In this section one of the optimal composite material designs (namely the high contrast E_r=8/ρ_r=4 one) is used to form a portion of a finite structure in order to examine shock-resistance performance at the structural level, and as an additional aim, to study the effect of damping. The material properties used are identical to those used in Section 2.1.

The structure considered is shown in Fig. 6. Its bottom half is composed of the periodic material with a 6x3 cell layout. Using the definition given in Eq. (8), and with the material properties known, the cell dimensions in this finite structure are chosen in a manner such that the excitation frequency is mapped to the frequency range of the first six dispersion branches. The structure has a square shape with a side length of 0.12m. With regard to damping, the type chosen is simple proportional (Raleigh) damping, i.e.,

$$\mathbf{C} = \alpha\mathbf{K} + \beta\mathbf{M}. \quad (15)$$

In this study α=0 and β is varied from 0 to 200×10^3. A finite element model was generated for this structure as shown in Fig. 6. A total of 14400 4-noded bilinear quadrilateral elements were used.

At the point marked "X" an excitation representing a shock load is applied as a prescribed displacement. This prescribed displacement was chosen to take the form of a double-Gaussian function

$$f_{DG}(t) = e^{-a(bt-c)^2} - e^{-a(bt-d)^2}, \quad (16)$$

where *a*, *b*, *c* and *d* are parameters. In order to synthesize a f_{DG} signal with a frequency content that approximately spans the range of interest, the parameters were chosen as follows:

$$a = 200,\ b = 1\text{x}10^4,\ c = 0.25,\ d = 0.26. \qquad (17)$$

This signal was chosen to demonstrate the feasibility of the proposed broadband frequency isolation design approach.

Explicit time integration was carried out using a time step of $\Delta t = 1.447\times10^{-7}$s over 500 steps. The displacement time history at a downstream point representing an "output" location (marked with a thick dot in Fig. 6) was recorded over the total time space of the simulation. It should be noted that the homogeneous region at the top side of the structure is included so that no wave interferences, at the output point, resulting from boundary reflections are experienced during the simulation time. This condition is imposed since the aim of this exercise is to test the transmissibility of only the synthesized periodic region of the structure.

In addition to examining the band-gap structure shown in Fig. 6, two parallel sets of simulations were carried out on totally homogeneous structures made out of the two extreme material phases, i.e., one has low stiffness/density, and the other has high stiffness/density. These simulations are used as benchmark cases to compare the performance of the designed structures with.

A summary of the results for all simulations performed is presented in Fig. 7. Shown is the maximum output displacement $u_{\text{o,max}}$, normalized by the maximum output displacement in the high stiffness/density structure, $u^{\text{H}}_{\text{o,max}}$. The figure clearly shows that the optimal band-gap structure produces significantly less output vibration response compared to the two homogeneous structures with extreme properties. Damping improves the isolation capacity of all structures, with the optimal and low stiffness/density homogeneous structures matching in capacity at high damping values (within the range considered).

5. CONCLUDING REMARKS

A genetic algorithm was employed for the design of two-dimensional periodic materials for a maximized sum of *SH*-mode band-gap widths across the first six branches. An array of optimal unit cell designs was generated for a range of Young's modulus and density ratios. The lower contrast cases tend to consist of hollow high stiffness/density inclusions while the higher contrast cases tend to produce solid inclusions. An increase in the density ratio is more effective in producing multiple band gaps than an increase in the Young's modulus which is effective in producing wide single band gaps. With regard to the landscape of the objective values, the total sum of the relative band-gap widths increases with material contrast. The increase takes place almost linearly with E_{r} and ρ_{r} with the rate of increase with E_{r} growing as ρ_{r} is increase and vice versa.

The optimal cell for the highest material contrast case was used to test broadband vibration isolation performance at the structural level. The effects of material damping were also considered. The results clearly demonstrate that enhanced structural performance will be attained when optimal band-gap materials such as those generated in this study are used for applications requiring broadband frequency isolation.

6. REFERENCES

[1] Cao, W.W. and Qi, W.K., 1995, "Plane-wave Propagation in Finite 2-2-Composites," *Journal of Applied. Physics*, Vol. **78**, pp. 4627-4632.

[2] Jensen, J.S., 2003, "Phononic Band Gaps and Vibrations in One- and Two-Dimensional Mass-Spring Structures," Journal of Sound and Vibration, Vol. **266**, pp. 1053-1078.

[3] Hussein, M.I., Hulbert, G.M. and Scott, R.A., 2003, "Band-Gap Engineering of Elastic Wave Guides Using Periodic Materials," *Proceedings ASME International Mechanical Engineering Congress and R&D Expo* (Washington, D.C., November 2003), ASME Publication, pp. 799-807.

[4] Hussein, M.I., Hulbert, G.M. and Scott, R.A., 2006, "Dispersive Elastodynamics of 1D Banded Materials and Structures: Analysis," *Journal of Sound and Vibration*, Vol. **289**, pp. 1053-1078.

[5] Cox, S.J. and Dobson, D.C., 1999, "Maximizing Band Gaps in Two Dimensional Photonic Crystals," *SIAM Journal Applied Mathematics*, Vol. **59**, pp. 2108-2120.

[6] Sigmund, O. and Jensen, J.S., 2003, "Systematic Design of Phononic Band-Gap Materials and Structures by Topology Optimization," *Philosophical Transactions of the Royal Society of London A*, Vol. **361**, pp. 1001-1019.

[7] Hussein, M.I., Hamza, K., Hulbert, G.M., Scott, R.A. and Saitou, K., 2004, "Evolutionary Topology Optimization of Periodic Materials for Vibration and Shock Isolation," *Proceedings 8th International Conference on Production Engineering, Design and Control*, (Alexandria University, Alezandria, Egypt, December, 2004), [CD ROM: pp. 1-10].

[8] Gazonas, G.A., Weile, D.S., Wildman, R. and Mohan, A., 2006, "Genetic algorithm optimization of phononic bandgap structures," *International Journal of Solids and Structures*, Vol. **43**, pp. 5851-5866.

[9] Hussein, M.I., Hulbert, G.M. and Scott, R.A., 2002, "Tailoring of Wave Propagation Characteristics in Periodic Structures with Multilayer Unit Cells," *Proceedings 17th American Society of Composites Technical Conference* (West Lafayette, Indiana, October 2002), CRC Press, [CD ROM: pp. 1-9].

[10] Hussein, M.I., Hamza, K., Hulbert, G.M., Scott, R.A. and Saitou, K., 2006, "Multiobjective evolutionary optimization of periodic layered materials for desired wave dispersion characteristics," *Structural and Multidisciplinary Optimization*, Vol. **31**, pp. 60-75.

[11] Dobson, D.C., 1999, "An Efficient Method for Band Structure Calculations in 2D Photonic Crystals," *Journal of Computational Physics*, Vol. **149**, pp. 363-376.

[12] Hussein, M.I., "Dynamics of Banded Materials and Structures: Analysis, Design and Computation in Multiple Scales," Ph.D. Thesis, Univeristy of Michigan, Ann Arbor, 2004.

[13] Brillouin, L., "Wave Propagation in Periodic Structures," 2nd edition, Dover, New York, 1953.

[14] Goldberg, D. "Genetic Algorithms in Search Optimization and Machine Learning," Addison – Wesley Publishing Company, 1989.

[15] Michalewicz, Z. "Genetic Algorithms + Data Structures = Evolution Programs," 3rd edition, Springer-Verlag, Berlin, Heidelberg, New York, 1996.

[16] Saab, Y. and Rao. V., 1990, "Stochastic Evolution: A Fast Effective Heuristic for Some Genetic Layout Problems," *Proceedings 27th ACM/IEEE Design Automation Conference*, pp. 26-31.

Table 1. Summary of genetic algorithm run parameters

Population Size	50
Number of Generations	30
Crossover Probability	0.99
Mutation Probability	0.02
Maximum iterations of local search	5

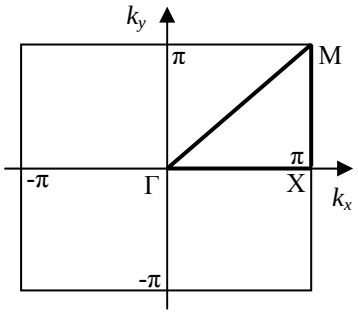

Figure 1. Unit cell domain and irreducible Brillouin zone (triangle) with the border symmetry points Γ, X and M marked.

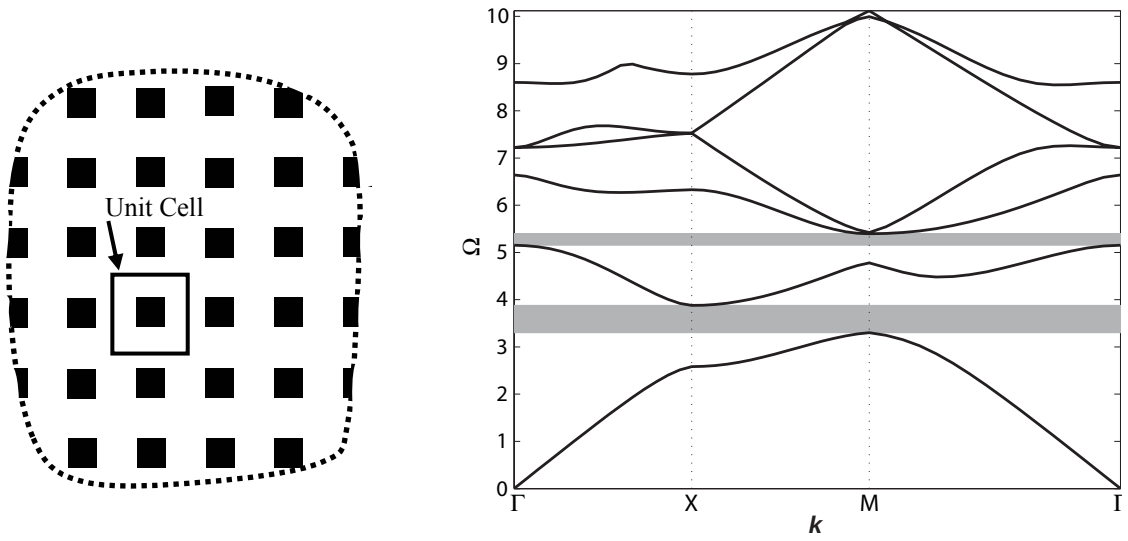

a b

Figure 2. a. Periodic composite material consisting of a low (white) and a high (black) stiffness/density material, respectively. A unit cell is marked. **b.** Frequency spectrum for out-of-plane *SH*-mode wave motion.

Figure 3. Optimal unit cell designs for a range of Young's modulus ratio and density ratio. The low and high stiffness/density material phases are represented with the white and black colors, respectively.

Figure 4. Optimal dispersion curves for a range of Young's modulus ratio and density ratio. Band gaps are shaded in grey.

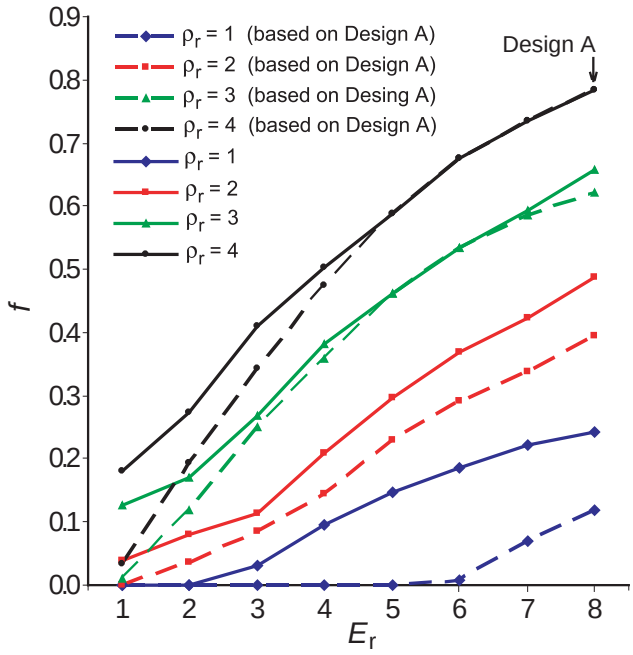

Figure 5. Optimal value of objective function for all the Young's modulus ratio and density ratio combinations considered. The dashed curves present an evaluation of the objective function based on Design A, which is the optimal design for E_r=4 and ρ_r=4.

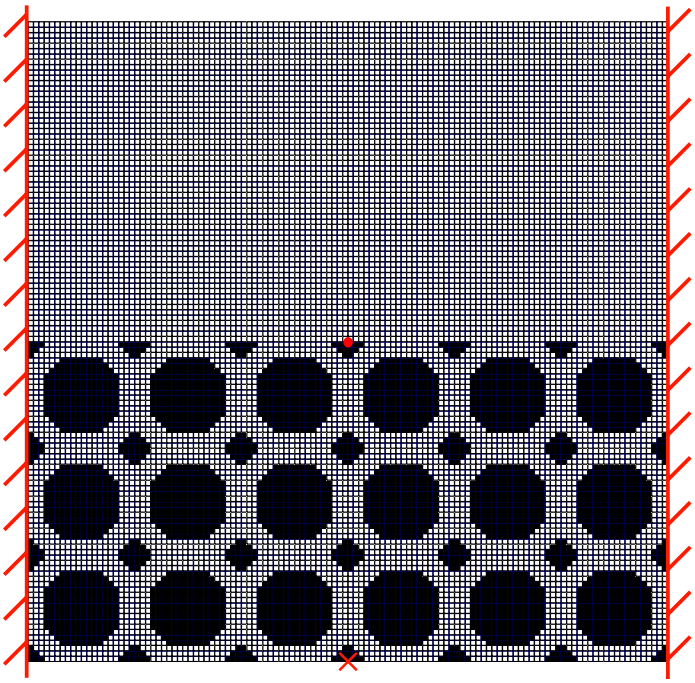

Figure 6. Finite structure with finite element mesh superimposed. The cell design used is the optimal design for $E_r=8/\rho_r=4$. The structure is clamped at the left and right edges and free at the remaining two edges. The excitation is applied at the point "X" and the response is measured at the pointed marked with a thick dot.

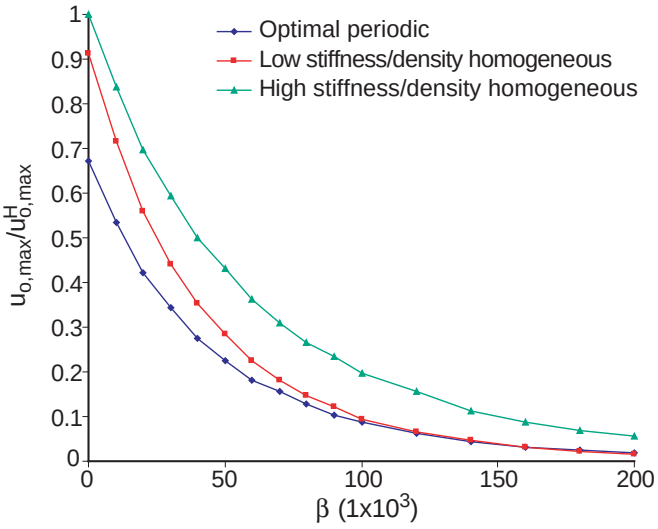

Figure 7. Maximum temporal response at the output point versus damping strength for a structure partially consisting of the designed band-gap composite (as shown in Fig. 6) and for a homogeneous structure composed of the low stiffness/density material and the high stiffness/density material, respectively. The response is normalized with respect the maximum temporal response at the output point for the high stiffness/density structure.